Fermi resonance in the Raman spectrum of the Se-vacancy breathing mode of MnGa$_2$Se$_4$

P. Alonso-Gutiérrez and M. L. Sanjuán*

Instituto de Ciencia de Materiales de Aragón (Universidad de Zaragoza-CSIC), Facultad de Ciencias,
Universidad de Zaragoza, 50009 Zaragoza, Spain

We present a Raman study of anharmonic phonon-lifetime broadening in MnGa$_2$Se$_4$, an ordered-vacancy compound with defect chalcopyrite structure. Contrary to the well studied zinc-blende compounds, defect chalcopyrites present 13 Raman active phonons, which allow for the detection of anharmonic effects in phonons of symmetry other than Γ_{15}. In this work, we focus on the Γ_1 breathing mode of the Se tetrahedron around the vacancy, an intense characteristic feature of all OVCs, found at 135 cm^{-1} in MnGa$_2$Se$_4$. The temperature dependences of the energy, linewidth, and asymmetry of the breathing mode are explained as due to anharmonic coupling with a two-phonon continuum. Within that model, the fit of the spectrum as a function of temperature provides the evolution of the bare single- and two-phonon coupled excitations, as well as that of the coupling parameter. A residual linewidth of about 0.2 cm^{-1}, not accounted for by the anharmonic decay model, is attributed to the Se isotope-mass fluctuation contribution.

I. INTRODUCTION

Ordered-vacancy compounds (OVCs) of type AB_2C_4 are promising materials for optoelectronic applications due to their unique combination of properties such as optical and structural anisotropy, noncentrosymmetry, high optical nonlinearity, etc., some of which are absent in the closely related compounds of the cubic zinc-blende structure.[1] One of the most interesting properties of OVC is the possibility to tune the electronic gap in a wide energy range with appropriate substitutions. If these include magnetic ions, dilution controlled magnetic and magneto-optic properties must be added to the preceding list.

Some technological applications of semiconductors depend on their carrier lifetimes, and these can be shortened by carrier-phonon interactions which, in turn, depend on phonon lifetimes.[2] Among other techniques, Raman scattering is suitable to study phonon lifetimes through the relation between mode linewidth Γ and lifetime τ, $1/\tau = 2\pi c\Gamma$ where c is the speed of light in cm/s and Γ is the full width at half maximum in cm^{-1}, provided that instrumental broadening is dealt with accurately. In addition, the temperature dependence of phonon linewidths yields information on phonon decay mechanisms.

Anharmonic decay results in line broadening. If the decaying phonon is close to a peak in the second-order density of states, third-order anharmonic decay can also show up as an asymmetric shape or even a structured band with enhanced intensity in the region of the two-phonon peak. This situation, known as the Fermi resonance,[3,4] is commonly found in zinc-blende compounds such as GaP,[5] ZnS,[6] and copper halides[4,7] and involves the interaction of either TO or LO modes with second-order excitations of near-zone-boundary phonons.

Although much work has been made on the phonon decay in zinc-blende semiconductors, very little is reported in ternary semiconductors such as chalcopyrite and ordered-vacancy compounds. In this work, we perform a Raman study of the anharmonic processes yielding asymmetry in

MnGa$_2$Se$_4$, an OVC of the A(II)B(III)$_2C$(VI)$_4$ family with a defect chalcopyrite structure.[8,9] In this lattice (see Fig. 1), all atoms are in quasitetrahedral coordination, with the peculiarity that ordered vacancies are found at specific crystallographic sites, so that the tetrahedron around a given Se atom is formed by 2Ga+Mn+vacancy. We focus, in particular, on the Se-vacancy breathing mode, a mode characteristic of all OVCs that usually appears as the strongest of the spectrum.[10] A broadening mechanism is proposed in terms of the coupling between the breathing mode and a second-order phonon continuum. Within such model, an expression for the profile is given and used to fit the temperature evolution of the spectrum. Physically relevant quantities are obtained, such as the interaction coefficient and the bare phonon and continuum frequencies. The strength of the process is explained in terms of the coincidence of two factors: a highly anharmonic potential affecting the Se-vacancy breathing mode, due to the presence of an ordered array of vacancies in the defect chalcopyrite structure, and the high density of states of 2TA(X) modes in zinc-blende compounds, which, in turn, is due to the flatness of the TA band near the X point.[11–13]
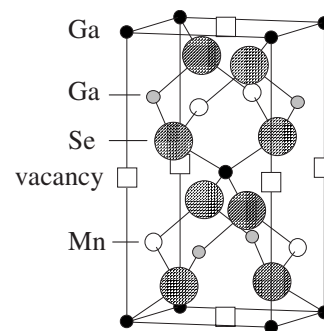
FIG. 1. Tetragonal unit cell of MnGa$_2$Se$_4$ with defect chalcopyrite structure (I-4 s.g.).
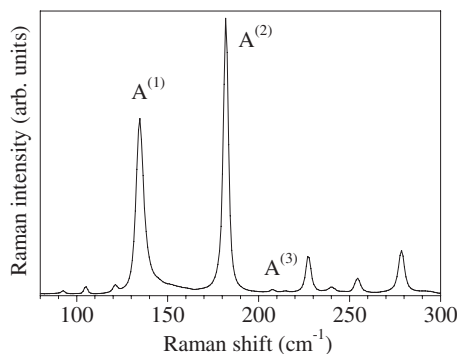
FIG. 2. Raman spectrum of a MnGa$_2$Se$_4$ single crystal measured at RT in backscattering configuration onto a (112) plane, with incident and scattered electric fields parallel to the [110] direction. λ =514.5 nm.

II. EXPERIMENTAL DETAILS

Small triangular shaped monocrystalline samples (about 2 mm side length) have been produced by the chemical vapor transport technique, using iodine as a transport agent.[14] Structural,[15] optical,[16] and Raman[17–19] characterization of our samples can be found in previous works. Raman measurements were performed in backscattering geometry in a Dilor XY spectrometer with a liquid-nitrogen-cooled charge-coupled device detector and excitation through a 50$\times$ microscope objective lens, using the 514.5 nm line of an Ar$^+$ laser. The Si mode at 520 cm^{-1} was used for frequency calibration. Power at the sample was $\approx$1 mW, and the spectral resolution $\approx$1.6 cm^{-1}. For low temperature measurements, a SMC-TBT cryostat was used.

III. EXPERIMENTAL RESULTS

Figure 2 shows the RT spectrum of MnGa$_2$Se$_4$ recorded for a (112) plane in backscattering geometry with incident and scattered electric fields parallel to the [110] direction. According to the I-4 symmetry of the defect chalcopyrite structure, MnGa$_2$Se$_4$ has 13 Raman active modes ($3A+5B$ $+5E$), all of which have been identified in a previous work.[17] The three A modes involve exclusively Se vibrations and are labeled in Fig. 2 as $A^{(1)}$, $A^{(2)}$, and $A^{(3)}$ in order of increasing energy. Normal coordinates for these modes can be found in Ref. 20. The appearance of a totally symmetric mode with high intensity is characteristic of all OVCs and is attributed to the breathing vibration of the Se tetrahedron toward the vacancy. In MnGa$_2$Se$_4$, it can be identified as the mode labeled $A^{(1)}$ with ω_1=135 cm^{-1} at RT. The second A mode, $A^{(2)}$, at ω_2=182 cm^{-1}, is active only in I-4 compounds and its intensity is usually much smaller than that of $A^{(1)}$, with the exception of MnGa$_2$Se$_4$. For completeness, we also display in Fig. 2 the third A mode $A^{(3)}$, which is very weak in all OVCs.

In this work, we shall focus on the shape and temperature behavior of the Se-vacancy breathing mode $A^{(1)}$. As Fig. 2 shows, it presents a remarkable asymmetry at RT. The asymmetry was found to be independent of the excitation wave-
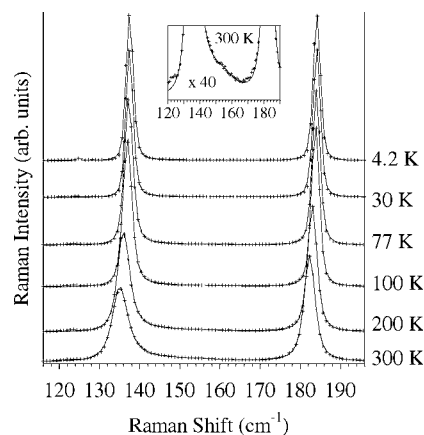
FIG. 3. Temperature evolution of the Raman spectrum of MnGa$_2$Se$_4$ in the region of the $A^{(1)}$ ($\omega \approx 135$ cm^{-1}) and $A^{(2)}$ ($\omega \approx 182$ cm^{-1}) modes. Crosses are the experimental data; the lines are the spectra calculated within the model of anharmonic coupling between the $A^{(1)}$ mode and a second-order phonon continuum, with the parameters given in the text. The $A^{(2)}$ mode is added to account for its contribution to the high frequency wing of the $A^{(1)}$ profile. The inset shows the region of the two-phonon continuum at RT.

length (from 1.96 to 2.71 eV), as well as of the direction of incident or scattered electric field polarization. Spectra on different crystallographic planes were also recorded, with the same result.

From our experiments, the only physical magnitude affecting the $A^{(1)}$ asymmetry is temperature. Figure 3 shows the T dependence of the spectrum, from 4 to 300 K, in the region of $A^{(1)}$ and $A^{(2)}$ modes. A weak B mode at 120 cm^{-1} is also present in this configuration. In Fig. 4, the T dependence of $\omega = \omega(A^{(1)})$ is compared to those of $A^{(2)}$ (ω_2) and of an E mode at 77 cm^{-1}. While the latter is only weakly dependent on T, both ω_1 and ω_2 show comparable down shifts of 2–2.5 cm^{-1} between liquid helium temperature (LHeT) and RT. More interesting is the linewidth evolution shown in Fig. 5. $A^{(1)}$ shows a remarkable broadening as compared to all other modes [data for $A^{(2)}$ and $E(77)$ are shown for refer-
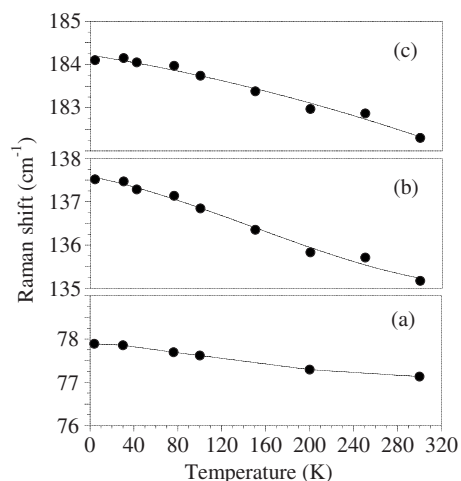
FIG. 4. Temperature evolution of the Raman shifts (peak positions) of (a) the $E(77)$, (b) the $A^{(1)}$, and (c) the $A^{(2)}$ modes.
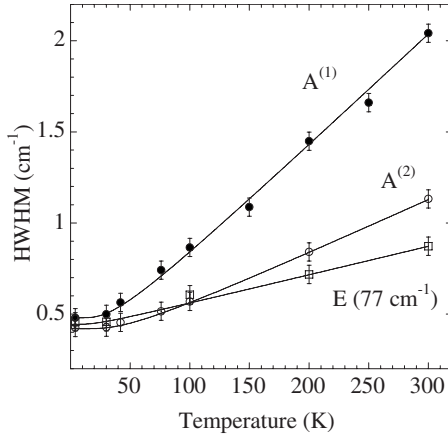
FIG. 5. Temperature evolution of the HWHM of the $E(77)$, $A^{(1)}$, and $A^{(2)}$ modes. The symbols are the experimental data, deconvoluted from instrumental broadening effects, and the lines are the fit of the data to expressions of type $\gamma + \Gamma_0[2n(\omega_i, T) + 1]$ with parameters given in the text.

ence] and its asymmetry, defined as the difference between the right and left half widths, increases significantly with temperature.

In the following section, we propose an explanation for the asymmetry of the $A^{(1)}$ mode as due to the anharmonic coupling of the mode with a two-phonon continuum. Based on this model, we perform a profile fitting to obtain physically relevant parameters such as the coupling strength and the bare mode frequencies as a function of temperature. The origin of the continuum and of the strong coupling is finally discussed in terms of phonon dispersion relations of zinc-blende compounds.

IV. MODEL AND DISCUSSION

From the possible sources of line broadening and/or asymmetry, structural disorder, either long or short range, can be ruled out in $MnGa_2Se_4$ since in this defect chalcopyrite, all cations and vacancies are ordered at specific crystallographic sites.[15] In agreement with this assertion, the Raman spectrum shows well resolved narrow peaks, typical of well ordered crystalline systems.

A common source of asymmetric broadening in Raman spectra is the coupling between a discrete excitation, usually a phonon or an electronic one, and a continuum of states, which can also have a phononic or an electronic origin. In simplest cases, the continuum is assumed to be constant and thus the mode adopts the well-known Fano profile, which is given by[21]

$$I(E) \propto \frac{(\varepsilon + q)^2}{(1 + \varepsilon^2)}, \qquad (1)$$

where $\varepsilon = (E - E_d)/\Gamma$, E_d being the energy of the discrete state, and Γ its lifetime. The parameter q determines the asymmetry degree: for high $|q| \gtrsim 10$ the profile is indistinguishable from a Lorentzian one; as $|q|$ gets smaller, the line becomes increasingly asymmetric, until a symmetric dip is reached for $|q| = 0$.

We have tried to fit the $A^{(1)}$ mode line shape to a Fano-like profile, with no success: Eq. (1) gives unphysically high intensity in the band tail toward which the asymmetry extends. Therefore, the hypothesis of a constant continuum was abandoned and we started from a more general expression for the Raman profile in the presence of interference between discrete and continuum states, such as the one given by Klein in Ref. 22,

$$I(E) = \frac{T_c^2}{\pi} \frac{\pi\rho(E)(E_d - E - VT_d/T_c)^2}{[E_d - E + V^2 R(E)]^2 + [\pi\rho(E)V^2]^2}. \qquad (2)$$

In this expression, E_d and T_d^2 are the energy and Raman activity of the discrete state, respectively, T_c^2 is the Raman activity of the continuum states and V is the parameter of coupling between discrete and continuum states. We assume V and T_c to be independent of E, i.e., all states from the continuum are equally Raman active and couple with the discrete state with the same strength. The continuum is characterized by its density of states $\rho(E) = \pi^{-1} \operatorname{Im}[g(E)]$ together with its Hilbert or Kramers-Kronig transform $R(E) = -\operatorname{Re}[g(E)]$, $g(E)$ being the Green's function of the excitations forming the continuum. No assumption is made, up to this point, on the nature of the continuum.

In many cases, though Raman allowed, the continuum is weakly active and Eq. (2) can be simplified by making $T_c = 0$ to obtain

$$I(E) = \frac{T_d^2}{\pi} \frac{\pi\rho(E)V^2}{[E_d - E + V^2 R(E)]^2 + [\pi\rho(E)V^2]^2}, \qquad (3)$$

where we recognize a pseudo-Lorentzian form, with central position shifted from E_d by $V^2 R(E)$ and width given by $\pi\rho(E)V^2$.

Since there is no *a priori* reason to discard other contributions to the phonon linewidth, besides the coupling with the continuum, we have introduced an additional parameter γ to take into account such other processes and obtain

$$I(E) = \frac{T_d^2}{\pi} \frac{\pi\rho(E)V^2 + \gamma}{[E_d - E + V^2 R(E)]^2 + [\pi\rho(E)V^2 + \gamma]^2}. \qquad (4)$$

At this point, it is clear that a detailed knowledge of the origin and shape of the continuum would be required to work with Eqs. (2)–(4) properly.

Since $MnGa_2Se_4$ is a wide-gap semiconductor ($E_g \approx 2.5$ eV at RT),[16] there are no electronic excitations available with energy in the region 100–200 cm^{-1} where the A modes are observed. So we disregard the possibility that the continuum has an electronic origin. Moreover, the increase of the asymmetry with temperature suggests a phononic nature of the continuum. Since all first-order Raman active modes have been identified and no disorder-activated modes are expected in this compound, the multiphononic character of the continuum arises in a natural way, most probably consisting of second-order excitations from high-symmetry points.

Within this assumption, the process yielding the $A^{(1)}$ phonon asymmetry can be described as the anharmonic decay of the $A^{(1)}$ phonon to a two-phonon excitation. In fact, Eq. (3) is

analogous to that obtained for the Raman profile from the calculation of the phonon self-energy $\Sigma(\omega)$ in the presence of third-order anharmonic interactions,[23–26]

$$I(\omega) \propto \frac{\Gamma(\omega)}{[\omega_0 - \omega + \Delta(\omega)]^2 + [\Gamma(\omega)]^2},$$

with the correspondence $\Delta(\omega) = \mathrm{Re}[\Sigma(\omega)] = V^2 R(\omega)$ and $\Gamma(\omega) = \mathrm{Im}[\Sigma(\omega)] = V^2 \pi \rho(\omega)$, $-R(\omega)$ and $\rho(\omega)$ being the real and imaginary parts of the two-phonon Green's function.

There are no lattice-dynamics calculations for $MnGa_2Se_4$, so that the detailed form of the two-phonon density of states is unknown. Thus, instead of using the expression for a phonon continuum Green's function, we introduce a lifetime-broadened single excitation centered at ω_c,

$$g(\omega) = 2\omega_c/[\omega_c^2 - \omega^2 - i2\omega_c\gamma_c],$$

where γ_c is an *ad hoc* inverse lifetime. Then,

$$R(\omega) = -2\omega_c(\omega_c^2 - \omega^2)/[(\omega_c^2 - \omega^2)^2 + (2\omega_c\gamma_c)^2] \quad (5a)$$

and

$$\rho(\omega) = (2\omega_c)^2 \gamma_c/[(\omega_c^2 - \omega^2)^2 + (2\omega_c\gamma_c)^2]. \quad (5b)$$

In this way, the continuum is characterized by only two parameters: central position ω_c and linewidth γ_c. We have introduced these expressions into Klein's formulas to fit the experimental spectra of Fig. 3 as a function of temperature. There are initially seven fitting parameters: three for the phonon (T_d, ω_d, γ), three for the continuum $(T_c, \omega_c, \gamma_c)$, and the coupling strength V. In the course of the fitting, we found that good results could be obtained with no continuum activity; thus, we assumed $T_c = 0$. Furthermore, in Eq. (3) or (4), the activity of the discrete state, T_d^2, is factorized just to scale the spectrum intensity, so that it does neither affect the spectrum shape nor the rest of parameters.

To further reduce the number of parameters, we have determined the intrinsic linewidth γ by assuming, as in writing Eq. (4), that the experimental linewidth Γ_{expt} can be decomposed as $\Gamma_{\mathrm{expt}} = \Gamma_v + \gamma$, where Γ_v stands for the contribution of the anharmonic coupling to the linewidth and that the temperature dependence of Γ_v can be modeled, in a first approximation, by the expression for the third-order anharmonic decay, $\Gamma_v = \Gamma_0[1 + n(\omega_a, T) + n(\omega_b, T)]$.[23,24] Then,

$$\Gamma_{\mathrm{expt}} = \Gamma_0[1 + n(\omega_a, T) + n(\omega_b, T)] + \gamma. \quad (6)$$

In these expressions, ω_a and ω_b are the frequencies of the two phonons to which the decay takes place, thus satisfying the condition $\omega_a + \omega_b = \omega_0$, $n(\omega, T)$ is the Bose-Einstein factor, Γ_0 is a parameter proportional to the square of the coupling strength V, and γ accounts for any temperature-independent residual linewidth.

The solid line in Fig. 5 shows the fit of the experimental half-width (deconvoluted from instrumental broadening effects) to Eq. (6). A very good fit is obtained in the assumption of decay to two phonons of equal energy $\omega_a = \omega_b = \omega_0/2$ (Klemens channel[27]) with $\omega_0 = 137.5 \text{ cm}^{-1}$, the phonon frequency at LHeT. The other fitting parameters are $\gamma = 0.18 \pm 0.03 \text{ cm}^{-1}$ and $\Gamma_0 = 0.30 \pm 0.01 \text{ cm}^{-1}$. The quality of the fitting supports our hypothesis for the decay mechanism.
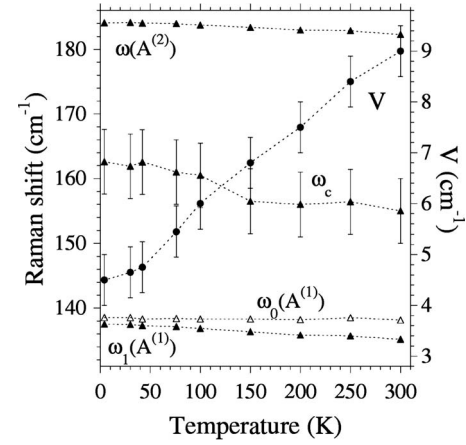
FIG. 6. Parameters derived from the fit of the spectrum. $\omega_1(A^{(1)})$ is the peak position of the $A^{(1)}$ mode and $\omega_0(A^{(1)})$ is its bare (quasi-harmonic) frequency. ω_c is the central position of the continuum and $V(T)$ the temperature-dependent coupling parameter. The experimental frequency of the $A^{(2)}$ mode is also included for comparison. Error bars (not shown) of ω_0, ω_1, and ω_2 are approximately $\pm 0.3 \text{ cm}^{-1}$.

Moreover, as we shall see later, the fact that the experimental linewidth follows a $2n+1$ law is important in the discussion of the origin of the second-order excitations forming the continuum.

We have used Eq. (4) to fit the spectra as a function of temperature with γ fixed at 0.2 cm^{-1} and only four fitting parameters: ω_d, ω_c, γ_c, and V. The $A^{(2)}$ mode was added to the spectrum to account for its contribution to the intensity in the high frequency tail of the $A^{(1)}$ mode. To account for instrumental broadening effects, the final step of our fitting procedure was always the convolution with a Gaussian function of the appropriate width, according to the slit used in the experiments (spectral half-width=0.84 cm^{-1}). The continuous lines in Fig. 3 are the result of the fitting. The inset in Fig. 3 shows a magnification of the RT spectrum to make evident the presence of the continuum as a shoulder of the $A^{(1)}$ band, as well as the quality of the fitting. We note that, since we have assumed that $T_c=0$, all the intensities in the region of the continuum stem from the coupling with the discrete phonon.

Figure 6 shows the experimentally determined $\omega_1(A^{(1)})$ together with the bare frequency $\omega_0(A^{(1)})$ obtained from the fitting. The central position of the continuum, ω_c, is also given, as well as the frequency of the $A^{(2)}$ mode, for comparison purposes. The temperature dependence of the bare (quasiharmonic) frequencies is due to thermal expansion. As shown in Fig. 6, this effect is negligibly small for the $A^{(1)}$ mode (ω_0 changes by no more than 0.5 cm^{-1} between 4 and 300 K, and the error in the determination of this parameter is ± 0.3 cm^{-1}). The difference $\Delta = \omega_0 - \omega_1$ is the coupling induced shift and varies from 1 to 3 cm^{-1} in the same temperature range.

The coupling parameter V is also represented in Fig. 6. Note that, as it is defined, V includes a temperature dependence from Bose-Einstein factors of $(2n+1)$ type. According to Eq. (4), the coupling provides a contribution to the line-

width given by $\Gamma_v = V^2 \pi \rho$. As discussed in Ref. 24, the correspondence between $V^2 \pi \rho + \gamma$ and the experimental linewidth is not exact, due to the ω dependence of $\rho(\omega)$ and $R(\omega)$ in the expression for the profile. In an approximate way,[24] the experimental linewidth can be related to $\Gamma_v + \gamma$ by the formula $\Gamma'_{expt} = (\Gamma_v + \gamma)/[1 - V^2 r_1(\omega_1)]$, where $r_1(\omega_1)$ stands for the first derivative of the function R taken at the renormalized phonon frequency ω_1. We have calculated $\Gamma_v + \gamma$ and compared it with Γ_{expt}. As expected, both sets of data deviate as T increases, but the divergence is almost within experimental error. Dividing by $1 - V^2 r_1$ makes the difference between Γ'_{expt} and Γ_{expt} almost negligible.

The presence of an intrinsic temperature-independent linewidth γ suggests that there is another mechanism, besides the anharmonic decay, contributing to the linewidth. To investigate if this behavior is general or due to a peculiarity of the $A^{(1)}$ phonon, we have performed the same kind of fitting for the $A^{(2)}$ and $E(77)$ modes, with the result that they also require the addition of a constant term $[\gamma(A^{(2)}) = 0.22 \pm 0.03 \text{cm}^{-1}, \gamma(E) = 0.4 \pm 0.05 \text{cm}^{-1}]$. Since $MnGa_2Se_4$ is crystallographically ordered, there are not many possibilities to explain the residual width, the most plausible one being the isotope-mass disorder.[28,29] Such effects have been observed in monatomic[30,31] and binary[30,32,33] semiconductors. In second order of mass fluctuation, the magnitude of the effect for a given phonon depends on the following factors:[28,29] the number and relative abundances of the isotopes of constituent elements, the contribution of each element to the eigenvector of that specific phonon (in the general case of multinary compounds), and the first-order phonon density of states at the frequency of the phonon under study projected onto the relevant sublattice.

In an OVC such as $MnGa_2Se_4$, the totally symmetric modes involve exclusively the anion vibrations, while both cations and anions may participate in B and E modes. Thus, in our case and for the $A^{(1)}$ or $A^{(2)}$ modes, only Se isotopes have to be taken into account, as in monatomic semiconductors. Natural Se has six isotopes, with the following masses and relative abundances of 74 (0.9%), 76 (9.4%), 77 (7.6%), 78 (23.8%), 80 (49.6%), and 82 (8.8%), yielding a mass variance factor[29] $g_2 \times 10^4 = 4.6$. However, as explained above, the isotope effect on the linewidth depends not only on mass variance but also on the value of the phonon density of states. The difference between $\gamma(A^{(1)}) = 0.18 \text{cm}^{-1}$ and $\gamma(A^{(2)}) = 0.22 \text{cm}^{-1}$ is small (in fact, it is within error), which suggests that the phonon densities of states at 135 and 182 cm^{-1} are quite similar in $MnGa_2Se_4$, tending to be higher at 182 cm^{-1}.

Having in mind that we have neither information on the phonon density of states of $MnGa_2Se_4$ nor on the eigenvectors of phonons other than the trivial totally symmetric ones, we can compare qualitatively the isotope effects found in $MnGa_2Se_4$ with those reported for zinc-blende compounds such as ZnSe and GaAs. In ZnSe, the contribution of isotope-mass fluctuations to the linewidth of the TO mode ($\omega_{TO} \approx 210 \text{ cm}^{-1}$) includes a contribution of both Zn ($g_2 \times 10^4 = 5.95$ for ^{nat}Zn) and Se elements.[32] At low temperature, and discounting the anharmonic broadening part, the isotope contribution to the full width is 1.4 cm^{-1} for samples

with natural Zn and Se composition and of about 0.4 cm^{-1} for a sample grown with pure ^{68}Zn isotope and maximum disorder in the Se sublattice.[32] Dividing by 2 to compare with our half-width at half maximum (HWHM) data, we see that our values for the $A^{(1)}$ and $A^{(2)}$ modes are very similar to those of the TO mode in ^{68}Zn^{dis}Se. On the other hand, in GaAs, only the Ga sublattice shows isotope disorder ($g_2 \times 10^4 = 1.97$ for ^{nat}Ga) since As is isotopically pure. Isotope effects in the HWHM of the TO mode of GaAs ($\omega_{TO} \approx 267 \text{ cm}^{-1}$) amount to only 0.06 cm^{-1}.[33]

As stated above, the temperature dependence of the asymmetric broadening of the $A^{(1)}$ mode suggests that the continuum has a phononic nature, most probably related to second-order excitations. The most intense contribution is expected to come from high-symmetry points of the reciprocal lattice. Since there are no lattice-dynamics calculations for $MnGa_2Se_4$, we shall, as a first approximation, look at the dispersion relations of zinc-blende compounds and relate them to OVC by means of the folding method.[9,34,35] This procedure has been widely used to discuss dispersion relations of ternary tetrahedral semiconductors. In Ref. 34, the assumption was made that the smaller the charge difference between constituent cations is, the closer the dispersion relations will be to those of zinc-blende parent compounds. In $MnGa_2Se_4$, the charge difference is of only $1e^-$, so that we assume the folding method to be valid, at least as a basis for the discussion.

From the binary compounds that may be considered as parents of $MnGa_2Se_4$ materials, Ga_2Se_3 is also an OVC and MnSe has a wurtzite structure. Among zinc-blende materials, the most closely related to $MnGa_2Se_4$, as regards lattice parameters and phonon frequency range, are ZnSe and GaAs. Then, we shall look at the dispersion relations of ZnSe and GaAs in the search of two-phonon excitations at $\approx 150 - 160 \text{ cm}^{-1}$, the range of the continuum central frequency obtained from the fitting.

By inspection of the reported experimental and calculated lattice dynamics of ZnSe and GaAs,[36,37] we find two kinds of phonon combinations that may yield energies in the range of $150 - 160 \text{ cm}^{-1}$: sum and difference processes. As for phonon differences, combinations yielding $\omega_a - \omega_b$ between 150 and 160 cm^{-1} can be found between optical and acoustic branches or between LA and TA ones. However, though in some cases these combinations may provide Γ_1 components,[38] they are discarded because the temperature dependence of such terms requires that they tend to 0 at low temperature and increase rapidly with T,[23,24] which is not the experimental observation for the $A^{(1)}$ mode. As shown in Fig. 5, the experimental linewidth can be very well explained by assuming that the decay takes place to a sum of two phonons of nearly equal energies.

Among sum combinations, only overtones of TA bands fulfill the energy and symmetry selection rules. In ZnSe, for instance, $\omega(TA_X) \approx 75 \text{ cm}^{-1}$, and in GaAs, $\omega(TA_X) \approx 80 \text{ cm}^{-1}$. Low-lying modes at W point appear between 80 and 100 cm^{-1} for ZnSe and between 100 and 114 cm^{-1} for GaAs.[36,37] TA(L) bands are too low in energy (between 50 and 60 cm^{-1}). In both compounds, strong peaks in the Γ_1 part of the two-phonon density of states (DOS) are found at

150–160 cm^{-1} arising from 2TA singularities.[11,13]

Overtones coming from zinc-blende TA bands in the vicinity of X or W points provide the correct Γ_1-type symmetry and a high DOS. In defect chalcopyrites, one X point and two W points are folded into Γ.[9] In particular, the low frequency X_5 mode yields the $E(77)$ mode, while the low-lying W_2 and W_4 modes are folded to yield another E mode at 105 cm^{-1} and two B modes at ≈ 90 and 120 cm^{-1}.[17] Due to the flatness of TA bands of zinc-blende compounds, acoustic phonons at the zone-boundary points of the folded Brillouin zone of OVC are expected to have energies still similar to those of zinc-blende compounds. Then, peaks in the two-phonon DOS at 150–160 cm^{-1} in MnGa$_2$Se$_4$ may come either from the folded zone center $E(77)$ mode or from TA branches near zone-boundary points with energy around 75–80 cm^{-1}.

We now discuss the similarities and differences between defect chalcopyrites and other compounds in relation with anharmonic coupling. Strong Fermi resonance effects have been observed in the Γ_{15} spectrum of zinc-blende compounds such as copper halides,[7] ZnS,[6] and GaP,[5] between the TO or LO zone center modes and acoustic phonon combinations. Similar effects have been reported for the E_2^{high} mode of wurtzite ZnO.[39]

Contrary to zinc-blende compounds, that do not have first-order Raman active modes of Γ_1 symmetry, in defect chalcopyrites, there exist totally symmetric zone center A modes, one of which involves the breathing vibration of Se atoms toward the structural vacancies. The presence of such vacancies favors a highly anharmonic vibrational potential for the Se-vacancy breathing mode. Moreover, in MnGa$_2$Se$_4$, the frequency of the breathing mode lies in the neighborhood (about 20 cm^{-1} apart) of an intense peak of the double-phonon density of states. Altogether, the anharmonicity of the lattice potential and the closeness of a high DOS with the appropriate symmetry in the same region favor the anharmonic coupling. This scenario is not exclusive of MnGa$_2$Se$_4$. As far as the condition of frequency proximity between the Se-breathing mode and the peak of the second-order DOS is fulfilled, similar or even stronger effects are expected in other OVCs.

V. CONCLUSION

We have reported a Fermi resonance in MnGa$_2$Se$_4$, an OVC of AB_2C_4 type. We provide an explanation for the occurrence of the coupling as due to both the anharmonic nature of the vibrational potential of the Se-vacancy breathing mode and the high density of two-phonon states arising from TA(X) overtones (in cubic notation).

Concerning phonon lifetimes, our model provides information about the anharmonic decay mechanism and its temperature dependence. The strong anharmonicity found for the vacancy-related mode is important in order to understand the consequences derived from the presence of empty cation sites. This, together with data on the two-phonon continuum, may also be of interest for lattice-dynamics studies of ordered-vacancy ternary semiconductors.

*Corresponding author; sanjuan@unizar.es

[1] A. N. Georgobiani, S. I. Radautsan, and I. M. Tiginyanu, Sov. Phys. Semicond. **19**, 121 (1985); L. K. Samanta, D. K. Ghosh, and P. S. Ghosh, Phys. Rev. B **39**, 10261 (1989); V. Petrov and F. Rotermund, Opt. Lett. **27**, 1705 (2002); M. C. Ohmer, R. Pandey, and N. H. Baraimov, MRS Bull. **23**, 16 (1998).

[2] M. A. Stroscio and M. Dutta, *Phonons in Nanostructures* (Cambridge University Press, Cambridge, 2001).

[3] J. Ruvalds and A. Zawadowski, Phys. Rev. B **2**, 1172 (1970).

[4] G. Kanellis, W. Kress, and H. Bilz, Phys. Rev. B **33**, 8733 (1986).

[5] F. Widulle, T. Ruf, A. Göbel, E. Schönherr, and M. Cardona, Phys. Rev. Lett. **82**, 5281 (1999).

[6] J. Serrano, A. Cantarero, M. Cardona, N. Garro, R. Lauck, R. E. Tallman, T. M. Ritter, and B. A. Weinstein, Phys. Rev. B **69**, 014301 (2004).

[7] M. Krauzman, R. M. Pick, H. Poulet, G. Hamel, and B. Prevot, Phys. Rev. Lett. **33**, 528 (1974); A. Göbel, T. Ruf, C. T. Lin, M. Cardona, J. C. Merle, and M. Joucla, Phys. Rev. B **56**, 210 (1997); J. Serrano, T. Ruf, F. Widulle, C. T. Lin, and M. Cardona, *ibid.* **64**, 045201 (2001).

[8] M. Cannas, L. Garbato, A. G. Lehmann, N. Lampis, and F. Ledda, Cryst. Res. Technol. **33**, 417 (1998).

[9] A. Miller, A. MacKinnon, and D. Weaire, Solid State Phys. **36**, 119 (1981).

[10] G. Attolini, S. Bini, P. P. Lottici, and C. Razzetti, Cryst. Res. Technol. **27**, 685 (1992).

[11] R. L. Schmidt, K. Kunc, M. Cardona, and H. Bilz, Phys. Rev. B **20**, 3345 (1979); D. N. Talwar, M. Vandevyver, K. Kunc and M. Zigone, *ibid.* **24**, 741 (1981).

[12] W. Weber, Phys. Rev. B **15**, 4789 (1977); B. D. Rajput and D. A. Browne, *ibid.* **53**, 9052 (1996).

[13] R. Trommer and M. Cardona, Phys. Rev. B **17**, 1865 (1978).

[14] F. Leccabue, B. E. Watts, C. Pelosi, D. Fiorani, A. M. Testa, A. Pajaczkowska, G. Bocelli, and G. Calestani, J. Cryst. Growth **128**, 859 (1992).

[15] M. C. Morón and S. Hull, Phys. Rev. B **64**, 220402(R) (2001).

[16] A. Millán and M. C. Morón, J. Appl. Phys. **89**, 1687 (2001).

[17] M. L. Sanjuán and M. C. Morón, Physica B **316-317**, 565 (2002).

[18] P. Alonso-Gutiérrez, M. L. Sanjuán, and M. C. Morón, Phys. Rev. B **71**, 085205 (2005).

[19] P. Alonso-Gutiérrez, M. L. Sanjuán, and M. C. Morón, *Physics of Semiconductors*, AIP Conf. Proc. No. 893 (AIP, New York, 2007), p. 185.

[20] H. Haeuseler, J. Solid State Chem. **26**, 367 (1978).

[21] U. Fano, Phys. Rev. **124**, 1866 (1961).

[22] M. V. Klein, in *Light Scattering in Solids II*, Topics in Applied Physics Vol. 50, edited by M. Cardona and G. Guntherodt

(Springer, Heidelberg, 1982).

[23] M. Balkanski, R. F. Wallis, and E. Haro, Phys. Rev. B **28**, 1928 (1983).

[24] J. Menéndez and M. Cardona, Phys. Rev. B **29**, 2051 (1984).

[25] G. Lang, K. Karch, M. Schmitt, P. Pavone, A. P. Mayer, R. K. Wehner, and D. Strauch, Phys. Rev. B **59**, 6182 (1999).

[26] A. Debernardi, Solid State Commun. **113**, 1 (2000); A. Debernardi, S. Baroni, and E. Molinari, Phys. Rev. Lett. **75**, 1819 (1995).

[27] P. G. Klemens, Phys. Rev. **148**, 845 (1966).

[28] S. Tamura, Phys. Rev. B **27**, 858 (1983); **30**, 849 (1984).

[29] M. Cardona and M. L. W. Thewalt, Rev. Mod. Phys. **77**, 1173 (2005).

[30] F. Widulle, J. Serrano, and M. Cardona, Phys. Rev. B **65**, 075206 (2002).

[31] J. M. Zhang, M. Giehler, A. Göbel, T. Ruf, M. Cardona, E. E. Haller, and K. Itoh, Phys. Rev. B **57**, 1348 (1998); A. Göbel, D. T. Wang, M. Cardona, L. Pintschovius, W. Reichardt, J. Kulda, N. M. Pyka, K. Itoh, and E. E. Haller, *ibid.* **58**, 10510 (1998).

[32] A. Göbel, T. Ruf, J. M. Zhang, R. Lauck, and M. Cardona, Phys. Rev. B **59**, 2749 (1999).

[33] F. Widulle, T. Ruf, A. Göbel, I. Silier, E. Schönherr, M. Cardona, J. Camacho, A. Cantarero, W. Kriegseis, and V. I. Ozhogin, Physica B **263-264**, 381 (1999).

[34] L. Artus, J. Pujol, J. Pascual, and J. Camassel, Phys. Rev. B **41**, 5727 (1990).

[35] A. Miller, D. J. Lockwood, A. Mackinnon, and D. Weaire, J. Phys. C **9**, 2997 (1976).

[36] B. Hennion, F. Moussa, G. Pepy, and K. Kunc, Phys. Lett. **36A**, 376 (1971).

[37] J. L. T. Waugh and G. Dolling, Phys. Rev. **132**, 2410 (1963); D. Strauch and B. Dorner, J. Phys. C **19**, 2853 (1986).

[38] W. G. Nilsen, Phys. Rev. **182**, 838 (1969).

[39] J. Serrano, F. J. Manjón, A. H. Romero, F. Widulle, R. Lauck, and M. Cardona, Phys. Rev. Lett. **90**, 055510 (2003).